

Universal crossover in surface superconductivity: Impact of varying Debye energy

Quanyong Zhu,¹ Xiaobin Luo,² A. A. Shanenko,^{3,4} and Yajiang Chen^{2,*}

¹*School of Mathematics and Computer Science, Lishui University, 323000 Lishui, China*

²*Zhejiang Key Laboratory of Quantum State Control and Optical Field Manipulation,*

Department of Physics, Zhejiang Sci-Tech University, 310018 Hangzhou, China

³*Moscow Center for Advanced Studies, Kulakova str. 20, Moscow 123592, Russia*

⁴*HSE University, 101000 Moscow, Russia*

(Dated: October 31, 2024)

Recently, interference-induced surface superconductivity (SC) has been predicted within an attractive Hubbard model with s -wave pairing, prompting intensive studies of its properties. The most notable finding is that the surface critical temperature T_{cs} can be significantly enhanced relative to the bulk critical temperature T_{cb} . In this work, considering a 1D attractive Hubbard model for the half-filling level, we investigate how this enhancement is affected by variations in the Debye energy $\hbar\omega_D$, which controls the number of states contributing to the pair potential and, in turn, influences the critical temperature. Our study reveals a universal crossover of the surface SC from the weak-to strong-coupling regime, regardless of the specific value of the Debye energy. The location of this crossover is marked by the maximum of $\tau = (T_{cs} - T_{cb})/T_{cb}$, which depends strongly on $\hbar\omega_D$. At its maximum, τ can increase up to nearly 70%. Additionally, we examine the evolution of the ratio $\Delta_{s0}/k_B T_{cs}$ along the crossover, where Δ_{s0} is the zero-temperature pair potential near the surface (the chain ends), and demonstrate that this ratio can significantly deviate from $\Delta_{b0}/k_B T_{cb}$, where Δ_{b0} is the zero-temperature bulk pair potential (in the chain center). Our findings may offer valuable insights into the search for higher critical temperatures in narrow-band superconductors.

I. INTRODUCTION

The physics of surface superconductivity (SC) has been a major focus in the fields of superconductivity and functional materials since the pioneering theoretical work by Saint-James and de Gennes [1]. Their work demonstrated that the surface SC persists at the magnetic fields between the second and third critical fields, a finding later confirmed in metallic alloys, such as $\text{Pb}_x\text{Tl}_{1-x}$ [2, 3], PbIn [4], PbBi [5] and NbTa [6]. At a certain field, the surface critical temperature T_{cs} , which is higher than the bulk critical temperature T_{cb} , is needed to destroy the surface SC. To characterize the surface enhancement, it is convenient to use the parameter $\tau = (T_{cs} - T_{cb})/T_{cb}$.

Additionally, other mechanisms of the surface SC enhancement not involving a magnetic field have been proposed, following Ginzburg's seminal work [7]. These predictions have been extensively investigated in both theory and experiments, including the surface SC induced by specific surface phonon modes [7–11], surface electron states [12, 13], and superconducting proximity effects [14–16].

Recently, a novel mechanism for the surface SC enhancement, induced by the near-surface constructive interference of itinerant quasiparticles in the absence of a magnetic field, was reported within the framework of the attractive Hubbard model with the nearest-neighbor hopping and s -wave pairing [17, 18]. (It is important to stress that the effect of interest does not arise within the parabolic band approximation [17, 19].) Its several nontrivial properties have been investigated. Notably, it

was shown that T_{cs} can be tailored by a weak external static electric field, while T_{cb} remains unchanged [20]. It was also demonstrated that this surface SC exhibits a Fulde-Ferrel-Larkin-Ovchinnikov state in external magnetic fields [21], shows significant enhancements at the sample corners in 2D and 3D cases [22], manifests a complex competition between itinerant quasiparticles and topological bound states in the proximitized topological insulators [23, 24], and persists in multiband superconductors [25].

It was also found that the surface SC is sensitive to the interplay between the pair coupling strength g and the chemical potential μ . In particular, it was shown [22] that the relative surface SC enhancement τ , taken as a function of g , exhibits a maximum dependent on μ . It was proved [26] that this feature appears in 1D, 2D, and 3D variants of the attractive Hubbard model, except for the situation with the chemical potential close to the band edges in the 1D case. The maximal value of τ is most pronounced in the 1D case, where τ was found to rise up to 25% for half-filling [26]. In the 2D and 3D cases, additionally to the surface SC, there are corner SC enhancements, where τ can go up to 40%, see Fig. 7 in Ref. 26.

However, the study in Ref. 26 was limited to the case where the Debye energy $\hbar\omega_D$ is larger than half the single-particle bandwidth, and did not explore the combined effects of varying both g and $\hbar\omega_D$ in the favored regime of half-filling. Reducing the Debye energy below half the bandwidth, modifies the number of quasiparticle states contributing to the pair potential, which can significantly influence the near-surface interference of the pair states. For instance, it was reported [27] that when $\hbar\omega_D$ goes below half the bandwidth, τ can increase to nearly 70%,

* yjchen@zstu.edu.cn

which is significantly larger than the results obtained in Ref. 26. Therefore, further investigations are required.

In the present work, we investigate how the interference-induced surface SC depends on both the coupling strength g and the Debye energy $\hbar\omega_D$ for half-filling. For simplicity, we focus on a 1D attractive Hubbard model with s -wave pairing. Our analysis is based on numerically solving the self-consistent Bogoliubov-de Gennes (BdG) equations, from which we extract the critical temperatures T_{cs} and T_{cb} , and then calculate τ . Our results reveal the presence of a universal crossover in the surface SC from the weak- to strong-coupling regimes, regardless of a particular Debye energy. This crossover is accompanied by a pronounced maximum of τ (up to nearly 70%), the value and position of which depend strongly on $\hbar\omega_D$. The corresponding ratio $\Delta_{s0}/k_B T_{cs}$ (where Δ_{s0} is the zero-temperature pair potential at the chain ends) deviates significantly from both its bulk counterpart and textbook BCS value. Throughout the paper, we use the term ‘‘surface’’ to refer to the behavior near the chain ends, maintaining a connection to higher dimensions, as our qualitative results on the surface SC are general and applicable to the 2D and 3D cases.

The paper is organized as follows. The BdG equations for a 1D attractive Hubbard model with s -wave pairing are outlined in Sec. II. Section III presents our results and discussions. Finally, concluding remarks are provided in Sec. IV.

II. THEORETICAL FORMALISM

As is mentioned in the Introduction, our consideration is based on a 1D attractive Hubbard model with s -wave pairing and nearest-neighboring hopping controlled by the amplitude t [17, 28]. The model Hamiltonian reads

$$H = - \sum_{i\sigma, \eta=\pm 1} t c_{i+\eta, \sigma}^\dagger c_{i\sigma} - \sum_{i\sigma} \mu c_{i\sigma}^\dagger c_{i\sigma} - g \sum_i n_{i\uparrow} n_{i\downarrow}, \quad (1)$$

where μ and g are the chemical potential and the pair coupling strength, respectively. $c_{i\sigma}$ and $c_{i\sigma}^\dagger$ are the annihilation and creation operators of an electron at the site i ($= 1, \dots, N$) with spin projection σ ($= \uparrow, \downarrow$), where N is the total site number. Additionally, $n_{i\sigma}$ is the site-dependent electron number operator. By applying the mean-field approximation [29], Eq. (1) is reduced to the effective mean-field Hamiltonian of the form

$$H_{\text{eff}} = \sum_{ij\sigma} H_{ij} c_{i\sigma}^\dagger c_{j\sigma} + \sum_i [\Delta(i) c_{i\uparrow}^\dagger c_{i\downarrow}^\dagger + \Delta^*(i) c_{i\downarrow} c_{i\uparrow}], \quad (2)$$

where $H_{ij} = -t(\delta_{i,j-1} + \delta_{i,j+1}) - \mu\delta_{ij}$, with δ_{ij} being the Kronecker delta function, and $\Delta(i)$ is the site-dependent superconducting pair potential. Notice that the Hartree-Fock potential is ignored in Eq. (2) as it merely introduces an extra confinement potential [30, 31] and does not qualitatively change our conclusions.

By diagonalizing H_{eff} with the Bogoliubov-Valatin transformation [32], the following BdG equations are obtained

$$\sum_j H_{ij} u_\alpha(j) + \Delta(i) v_\alpha(i) = \varepsilon_\alpha u_\alpha(i), \quad (3a)$$

$$\Delta^*(i) u_\alpha(i) - \sum_j H_{ij}^* v_\alpha(j) = \varepsilon_\alpha v_\alpha(i). \quad (3b)$$

Here, ε_α , $u_\alpha(i)$ and $v_\alpha(i)$ are the quasiparticle energy and wavefunctions, respectively. The self-consistent condition for $\Delta(i)$ is derived by comparing the free energies for the effective and full Hamiltonians, which results in

$$\Delta(i) = g \sum_{0 \leq \varepsilon_\alpha \leq \hbar\omega_D} u_\alpha(i) v_\alpha^*(i) [1 - 2f(\varepsilon_\alpha)], \quad (4)$$

with $f(\varepsilon_\alpha)$ being the Fermi-Dirac distribution function. The summation range in Eq. (4) indicates that only the physical branch of the quasiparticle spectrum should be taken into account [29]. Higher-energy quasiparticles contribute more significantly to the surface SC compared to lower-energy ones (strictly speaking in the absence of external electric fields, see Fig. 3 in Ref. [27]). This explains why the value of $\hbar\omega_D$ is so important in studying the surface SC.

In addition, when solving the BdG equations, one should take into consideration that the electron density $n_e(i)$ is also connected to the quasiparticle specifications by the relation

$$n_e(i) = 2 \sum_\alpha f(\varepsilon_\alpha) |u_\alpha(i)|^2 + [(1 - f(\varepsilon_\alpha)) |v_\alpha(i)|^2]. \quad (5)$$

This relation determines the chemical potential μ for a given electron filling level $\bar{n}_e = (1/N) \sum_i n_e(i)$.

To self-consistently solve the BdG equations (3), we begin by applying initial trial values for the pair potential $\Delta(i)$ and the chemical potential μ . These initial values are used to construct the matrix eigenvalue equation from the BdG equations given by Eq. (3). Solving this eigenvalue problem provides the corresponding quasiparticle spectrum and wavefunctions, from which updated values for $\Delta(i)$ and the electron density $n_e(i)$ are calculated according to Eqs.(4) and (5). Given a fixed electron filling level \bar{n}_e , a new μ can then be determined. The process continues iteratively, with the updated $\Delta(i)$ and μ being reinserted into the BdG equations, until both quantities converge according to the desired level of accuracy.

In our calculations, the hopping parameter t can be scaled out so that Δ , μ , ε_α , g , $\hbar\omega_D$, and the band width are measured in units of t . The temperature (along with T_{cs} and T_{cb}) is given in units of t/k_B , where k_B is the Boltzmann constant. The number of sites is set to $N = 301$, which is large enough to avoid quantum-size effects [30, 33]. Finally, the accuracy of the self-consistent calculation of $\Delta(i)$ and μ is set to 10^{-8} .

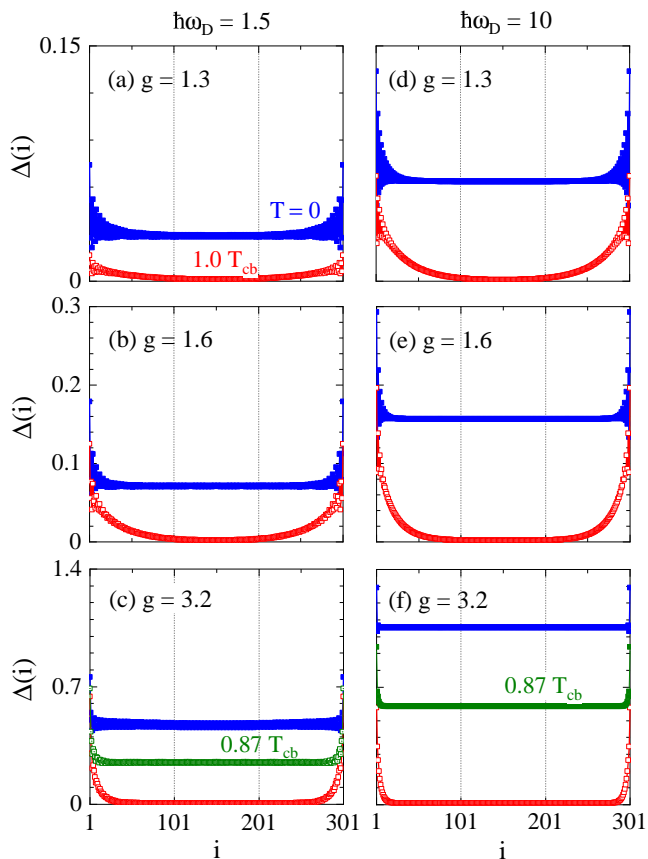


FIG. 1. The pair potential $\Delta(i)$ versus the site index i , as calculated for $g = 1.3, 1.6, 3.2$, with $\hbar\omega_D = 1.5$ (a-c), 10 (d-f). The blue curves represent data for $T = 0$, while the green and red ones are for $T = 0.87 T_{cb}$ and $1.0 T_{cb}$, respectively.

III. RESULTS AND DISCUSSIONS

To illustrate the influence of the coupling strength g and Debye energy $\hbar\omega_D$ on the surface SC, Fig. 1 shows profiles of the pair potential $\Delta(i)$ calculated for $g = 1.3, 1.6$, and 3.2 with $\hbar\omega_D = 1.5$ and 10 for several temperatures. The blue, green, and red curves represent data for $T/T_{cb} = 0, 0.87$, and 1.0 , respectively. For the bulk critical temperature, we have $T_{cb} = 0.020, 0.044$ and 0.290 for $g = 1.3, 1.6$, and 3.2 at $\hbar\omega_D = 1.5$, while $T_{cb} = 0.041, 0.095$, and 0.599 at $\hbar\omega_D = 10$. Here we deliberately choose the two typical scenarios: one is for the Debye energy larger than half the bandwidth 2 , while the other is for $\hbar\omega_D$ smaller than 2 . The last scenario means that all the physical branch quasiparticles are included in the summation of Eq. (4), while the first scenario implies significant limitations on the higher-energy quasiparticles.

At $T = 0$, all the pair potentials shown in Figs. 1(a-f) are enhanced near the chain ends ($i = 1$ and 301), which, in higher dimensions, corresponds to the surface SC. For both $\hbar\omega_D = 1.5$ and 10 at $T = 0$, the larger the value of g , the greater the pair potential near the boundaries (the surface pair potential). For the same value of g , the

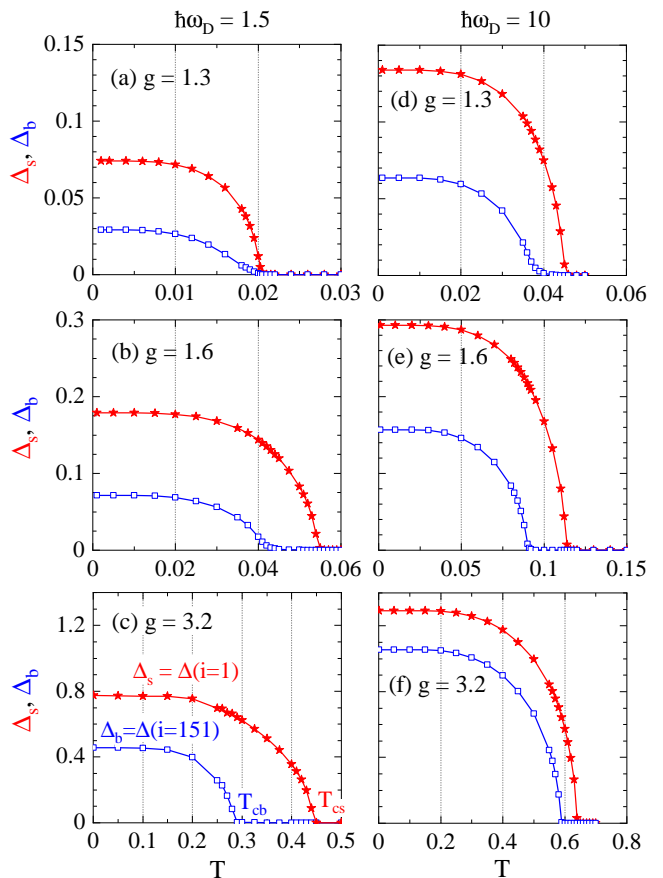


FIG. 2. The surface (at the chain ends; curves with red stars) and bulk (in the chain center; curves with blue squares) local pair potentials, $\Delta_s = \Delta(i = 1, \dots, 301)$ and $\Delta_b = \Delta(i = 151)$, are shown as functions of temperature T for $g = 1.3, 1.6$, and 3.2 , with $\hbar\omega_D = 1.5$ (a-c) and $\hbar\omega_D = 10$ (d-f). The surface and bulk critical temperatures (T_{cs} and T_{cb}), where Δ_s and Δ_b respectively drop to zero, are highlighted in panel (c).

surface pair potential for $\hbar\omega_D = 10$ is higher than that of $\hbar\omega_D = 1.5$, due to a larger number of the contributing quasiparticles in the case of $\hbar\omega_D = 10$. For all relevant parameters, the bulk pair potential (in the chain center) vanishes at $T/T_{cb} = 1.0$, while the surface pair potential remains finite at higher temperatures $T_{cb} < T < T_{cs}$. Figure 1 shows that the region with the zero pair potential around the center of the system increases as g rises. Consequently, the spatial extent (and the related characteristic length) over which the condensate near the boundaries persists decreases with increasing g .

In Fig. 2, the temperature-dependent surface and bulk pair potentials, $\Delta_s = \Delta(i = 1) = \Delta(i = N)$ and $\Delta_b = \Delta(i = 151)$, are presented for $g = 1.3, 1.6$, and 3.2 at $\hbar\omega_D = 1.5$ (a-c) and 10 (d-f). As T increases, both $\Delta_s(T)$ and $\Delta_b(T)$ decrease, eventually approaching zero at T_{cs} and T_{cb} , respectively. For $\hbar\omega_D = 1.5$, we find $T_{cs} = 0.0210, 0.0545$, and 0.445 at $g = 1.3, 1.6$, and 3.2 , respectively. The corresponding values of the surface SC enhancement parameter are calculated as

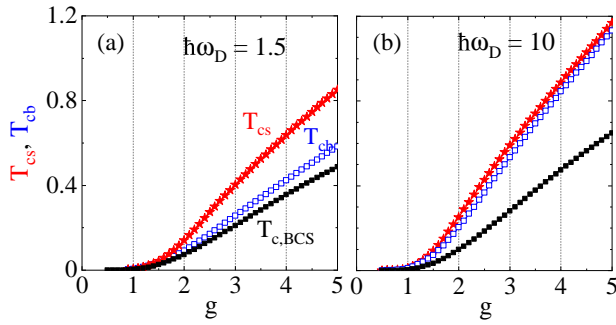


FIG. 3. T_{cs} and T_{cb} as functions of the coupling strength g for $\hbar\omega_D = 1.5$ (a) and 10 (b). The results of T_{cs} and T_{cb} are given by red-starred and blue-squared curves, respectively. The black curves with solid squares represent the BCS critical temperature $T_{c,BCS}$.

$\tau = 5.0\%$, 23.9% , and 53.4% . In this case, the higher the value of g , the greater the value of τ . For $\hbar\omega_D = 10$, we find $T_{cs} = 0.0455$, 0.115 , and 0.645 at $g = 1.3$, 1.6 , and 3.2 , with the corresponding surface SC enhancements of $\tau = 13.8\%$, 26.4% , and 9.3% , respectively. Unlike the case of $\hbar\omega_D = 1.5$, τ does not increase with g for $\hbar\omega_D = 10$. Thus, we conclude that variations in $\hbar\omega_D$ significantly affect the g -dependence of the surface SC enhancement parameter τ .

To delve deeper, Fig. 3 illustrates the surface and bulk critical temperatures as functions of the coupling strength g for $\hbar\omega_D = 1.5$ and 10. The red-starred curves represent the data for T_{cs} , while the blue-squared curves correspond to T_{cb} . Additionally, the black curves with solid squares depict the BCS critical temperature $k_B T_{c,BCS} = 1.134\hbar\omega_D e^{-1/gD(\mu)}$, with $D(\mu)$ being the normal single-electron density of states (DOS) [29]. $D(\mu)$ is extracted from the single-electron spectrum of the tight-binding model $\xi_n = -2t\cos(k_n a)$, with $k_n a = \pi n/(N+1)$, $n = 1, \dots, N$ and a being the lattice constant [28]. At $\mu = 0$, corresponding to half-filling, we have $k_n a = \pi/2$ and $D(\mu) = \frac{N+1}{N-1} \cdot \frac{1}{2\pi\sin(k_n a)} \approx 1/2\pi$ (DOS is in units of $1/t$). Since there are no single-electron states with $|\xi_n| > 2$, the pair potential does not change as $\hbar\omega_D$ increases above 2 [27]. Therefore, for the BCS critical temperature we adopt $\hbar\omega_D = 1.5$ in Fig. 3(a) and $\hbar\omega_D = 2$ in Fig. 3(b).

As shown in Fig. 3(a) with $\hbar\omega_D = 1.5$, the critical temperatures T_{cs} , T_{cb} , and $T_{c,BCS}$ remain close to zero for $g < 1$. They then exhibit an exponential-like increase in the region $1 < g < 2.5$, which is replaced by an almost linear growth with g in the domain $2.5 < g < 5$. Notably, for $g > 1.5$, we observe $T_{cs} > T_{cb} > T_{c,BCS}$. The difference between T_{cb} and $T_{c,BCS}$ is significantly smaller than the difference between T_{cs} and T_{cb} , indicating that T_{cb} behaves more similar to the BCS prediction compared to T_{cs} .

In Fig. 3(b) with $\hbar\omega_D = 10$, both T_{cs} and T_{cb} are higher than those shown in Fig. 3(a) with $\hbar\omega_D = 1.5$ for the corresponding coupling values. Although T_{cs} is

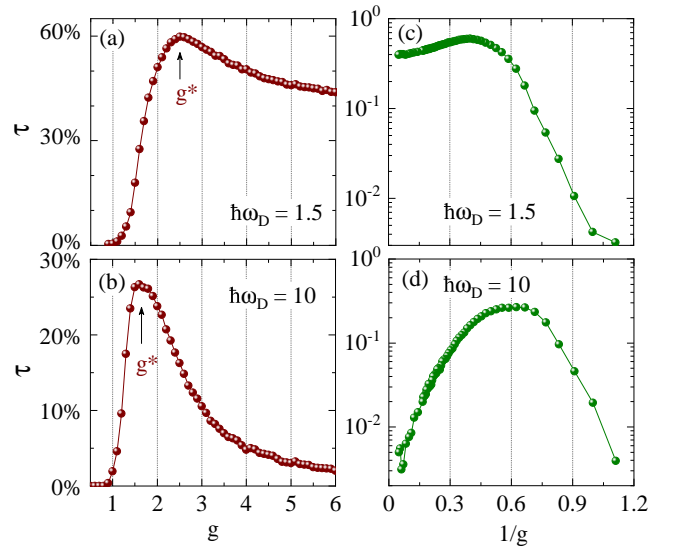


FIG. 4. The surface SC enhancement parameter $\tau\tau = (T_{cs} - T_{cb})/T_{cb}$ is presented as a function of the coupling strength g (a, b) and $1/g$ (c, d) for $\hbar\omega_D = 1.5$ and 10. Panels (c, d) employ a base-10 logarithmic scale to plot the data for τ . The location of the τ -maximum $g = g^*$ can be considered as the crossover point that distinguishes between the weak-coupling and strong-coupling behaviors of τ as a function of g .

still larger than T_{cb} in Fig. 3(b), the gap between them is much less than in panel (a). This indicates that a higher T_{cs} does not necessarily result in a greater surface SC enhancement parameter τ . The underlying physics arises from the complex interplay of higher- and lower-energy quasiparticles, which is sensitive to the Debye energy [20, 27]. Moreover, both T_{cs} and T_{cb} deviate significantly from the BCS behavior for $g > 1.5$, as they are much larger than $T_{c,BCS}$.

Now, we examine how the surface-SC enhancement parameter τ depends on the coupling strength g for $\hbar\omega_D = 1.5$ and 10, as shown in Fig. 4. Panels (a, b) present τ as a function of g for $\hbar\omega_D = 1.5$ and 10, respectively, while panels (c, d) use a base-10 logarithmic scale to plot the same data as a function of $1/g$, similar to how results for the BCS-BEC crossover are often displayed. For $\hbar\omega_D = 10$ in Fig. 4(b, d), τ is zero at $g < 1$, peaks at 26.7% when $g = g^* = 1.60$, and then decreases to zero as g increases beyond $g = g^*$. This qualitatively agrees with the results of Ref. [26], which shows that τ tends to zero in the strong-coupling regime for $\hbar\omega_D > 2$ (all the physical quasiparticles are included in the pair potential) and for various values of the chemical potential.

In contrast, for $\hbar\omega_D = 1.5$, one observes that τ is exponentially small as $g \rightarrow 0$, but increases significantly, reaching its maximum $\tau_{\max} = 60.0\%$ when g approaches $g^* = 2.5$. For $g > g^*$, τ gradually decreases as g increases but remains finite, approaching a saturation near 39.4% . This differs from the results of Ref. [26], highlighting the importance of investigating how the Debye energy influ-

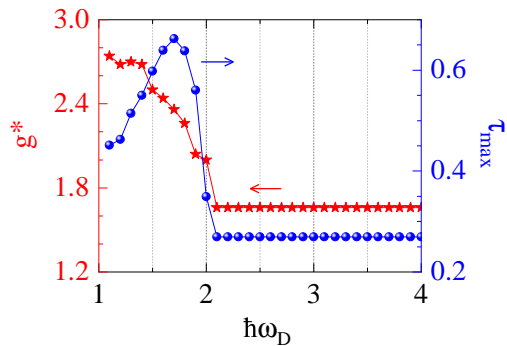


FIG. 5. The $\hbar\omega_D$ -dependence of the characteristics of the universal crossover in the surface SC, with g^* (curves with red stars) and τ_{\max} (curves with blue spheres) plotted as functions of $\hbar\omega_D$.

ences τ . Notably, the shape of the data in panels (a, c) resembles the behavior of the critical temperature in the BCS-BEC crossover [34, 35].

Figure 4 demonstrates a crossover in the g -dependence of the surface-SC enhancement parameter τ between qualitatively different weak- and strong-coupling regimes. This crossover is marked by a maximum of τ , denoted as τ_{\max} , which occurs at $g = g^*$. Although the crossover is universal and occurs at any value of $\hbar\omega_D$, its characteristics are strongly influenced by a value of the Debye energy. In particular, Fig. 5 demonstrates g^* and τ_{\max} as functions of $\hbar\omega_D$, which are given by red-starred and blue-sphere curves, respectively. One sees, that as $\hbar\omega_D$ increases from 1 to 2, g^* decreases, shifting toward the weak-coupling regime. For $\hbar\omega_D > 2$, the position of the maximum of τ remains unchanged with $\hbar\omega_D$, stabilizing at $g^* = 1.66$. In turn, τ_{\max} initially increases with $\hbar\omega_D$, reaching 66.3% at $\hbar\omega_D = 1.7$, and then it drops rapidly to 26.9%, remaining unchanged for $\hbar\omega_D > 2$. The peaked behavior of τ_{\max} in Fig. 5 appears because the most significant surface-SC contribution comes from the states with the quasiparticle energy $\varepsilon_\alpha = 1.7$.

Next, we focus on the g -dependence of the ratios $\Delta_{s0}/k_B T_{cs}$, where $\Delta_{s0} = \Delta(i = 1)$ is the zero-temperature surface (boundary) pair potential, and $\Delta_{b0}/k_B T_{cb}$, where $\Delta_{b0} = \Delta(i = 151)$ denotes the zero-temperature pair potential in the chain center (bulk). In Fig. 6, the red-starred and blue-squared curves represent Δ_{s0} and Δ_{b0} , respectively, as functions of g for $\hbar\omega_D = 1.5$ (a, b) and 10 (c, d). Additionally, the black-squared curve corresponds to the BCS result Δ_{BCS} , calculated as $\Delta_{\text{BCS}} = 2\hbar\omega_D e^{-1/gD(\mu)}$. Following the calculations for $T_{c,\text{BCS}}$ in Fig. 3, $\hbar\omega_D$ is taken as 1.5 for Δ_{BCS} in Fig. 6(a), while in Fig. 6(c), Δ_{BCS} is calculated with $\hbar\omega_D = 2$, as $\hbar\omega_D = 10$ exceeds half the bandwidth.

From Fig. 6(a), we observe that for $\hbar\omega_D = 1.5$, the zero-temperature pair potential in the chain center, Δ_{b0} , is nearly equal to the BCS estimate $\Delta_{0,\text{BCS}}$. In contrast, the zero-temperature pair potential at the chain ends, Δ_{s0} , is significantly higher than $\Delta_{0,\text{BCS}}$. However, for

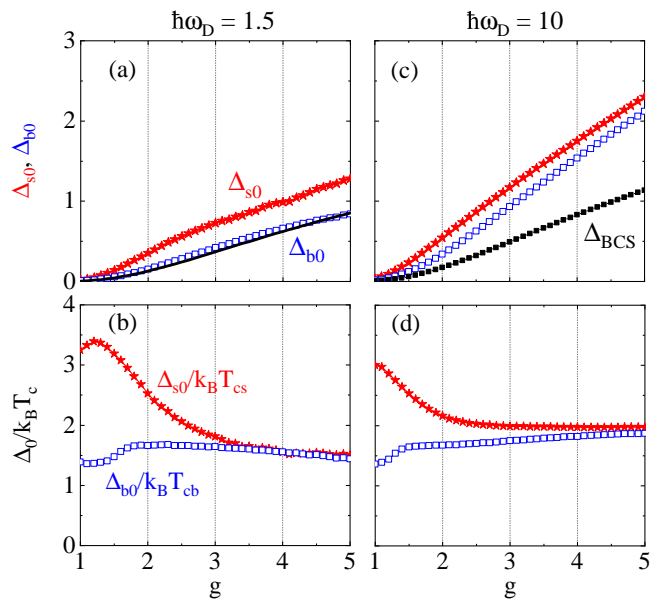


FIG. 6. Δ_{s0} and Δ_{b0} (a, c), and the ratios $\Delta_{s0}/k_B T_{cs}$ and $\Delta_{b0}/k_B T_{cb}$ (b, d) as functions of the coupling strength g for $\hbar\omega_D = 1.5$ (a, b) and 10 (c, d). The surface (for the chain ends) and bulk (for the chain center) results are given by curves with red stars and blue squares, respectively. The BCS estimates of the zero-temperature pair potential Δ_{BCS} are given by black curves with solid squares, see panels (a) and (c).

$\hbar\omega_D = 10$, which exceeds half the single-electron bandwidth, the difference from the BCS estimate becomes more pronounced: both Δ_{s0} and Δ_{b0} are much larger than $\Delta_{0,\text{BCS}}$.

Using the results from Figs. 3 and 6(a), we calculate $\Delta_{s0}/k_B T_{cs}$ and $\Delta_{b0}/k_B T_{cb}$ for $\hbar\omega_D = 1.5$ and 10, see Figs. 6 (b) and (d). For $\hbar\omega_D = 1.5$, Fig. 6(b) shows that $\Delta_{s0}/k_B T_{cs}$ increases with g in the region $1 < g < 1.2$, reaching a maximum value of 3.39 at $g = 1.2$. As g increases from 1.2 to 3.5, $\Delta_{s0}/k_B T_{cs}$ decreases rapidly, approaching at $g = 3.5$ the center-of-chain ratio $\Delta_{b0}/k_B T_{cb} = 1.646$, which is lower than the BCS value of about 1.76 [36]. For $g > 3.5$, both $\Delta_{s0}/k_B T_{cs}$ and $\Delta_{b0}/k_B T_{cb}$ exhibit a very slow, almost negligible decrease with increasing g .

The results for $\hbar\omega_D = 10$, shown in Fig. 6(d), are similar, with two minor differences. First, the maximum value of $\Delta_{s0}/k_B T_{cs}$ is around 3.00, which is lower than in panel (b). Second, both $\Delta_{s0}/k_B T_{cs}$ and $\Delta_{b0}/k_B T_{cb}$ slowly increase with g for sufficiently strong couplings, approaching 1.92, which is higher than the corresponding value for $\hbar\omega_D = 1.5$ and the textbook BCS result. Therefore, while $\Delta_{s0}/k_B T_{cs}$ significantly exceeds $\Delta_{b0}/k_B T_{cb}$ on the weak-coupling side of the crossover, they are very close to one another on the strong-coupling side. Notably, $\Delta_{s0}/k_B T_{cs}$ is always larger than the BCS ratio, and significantly exceeds it in the weak-coupling regime.

IV. CONCLUSIONS

By numerically solving the self-consistent Bogoliubov-de Gennes equations for a $1D$ attractive Hubbard model with s -wave pairing at half-filling, we have systematically investigated the combined effects of varying both the pair coupling g and the Debye energy $\hbar\omega_D$ on surface superconductivity (SC) enhancement. Our study reveals a universal crossover in surface SC from weak- to strong-coupling behavior, which occurs regardless of the specific value of $\hbar\omega_D$. This crossover is characterized by a maximum in the relative enhancement of the surface critical temperature, τ (the critical temperature at the chain end in our study), which can reach up to about 70%.

The characteristics of this crossover are highly sensitive to the Debye energy when it is below half the single-particle bandwidth, with the enhancement of surface SC being most pronounced in this case. While our study focuses on half-filling, similar results are expected beyond this condition, although the effect tends to diminish as the system deviates from half-filling [17, 22].

Although our investigation is based on a $1D$ model, a similar universal crossover can be expected at any value

of $\hbar\omega_D$ for $2D$ and $3D$ attractive Hubbard models, as can also be seen from conclusions of Ref. 22. In particular, the results of our model are applicable to the case of a Hubbard model describing an array of parallel chains with relatively small hopping amplitudes between them, see Ref. [37]. Moreover, this kind of universal crossover in the coupling dependence of the critical temperature could also be expected for corner SC enhancements in $2D$ and $3D$ cases, also reported for an attractive Hubbard model [22].

ACKNOWLEDGMENTS

This work was supported by the Science Foundation of Zhejiang Sci-Tech University (Grants No. 19062463-Y). A.A.S. thanks the Grant of Ministry of Science and Higher Education of the Russian Federation No. 075-15-2024-632 for the support that helped to perform investigations of the universal crossover in the interference-induced surface superconductivity. Analysis of numerical solutions of the formalism was supported by the HSE University Basic Research Program.

-
- [1] D. Saint-James and P. de Gennes, Onset of superconductivity in decreasing fields, *Physics Letters* **7**, 306 (1963).
 - [2] G. Bon Mardion, B. Goodman, and A. Lacaze, Le champ critique de la surface supraconducteur, *Physics Letters* **8**, 15 (1964).
 - [3] W. J. Tomasch and A. S. Joseph, Experimental Evidence for a new Superconducting Phase Nucleation Field in Type-II Superconductors, *Phys. Rev. Lett.* **12**, 148 (1964).
 - [4] S. Gygax, J. Olsen, and R. Kropschot, Four critical fields in superconducting indium lead alloys, *Physics Letters* **8**, 228 (1964).
 - [5] M. Strongin, A. Paskin, D. G. Schweitzer, O. F. Kammerer, and P. P. Craig, Surface Superconductivity in Type I and Type II Superconductors, *Phys. Rev. Lett.* **12**, 442 (1964).
 - [6] C. F. Hempstead and Y. B. Kim, Resistive Transitions and Surface effects in Type-II Superconductors, *Phys. Rev. Lett.* **12**, 145 (1964).
 - [7] V. Ginzburg, On surface superconductivity, *Physics Letters* **13**, 101 (1964).
 - [8] M. Strongin, O. F. Kammerer, J. E. Crow, R. D. Parks, D. H. Douglass, and M. A. Jensen, Enhanced Superconductivity in Layered Metallic Films, *Phys. Rev. Lett.* **21**, 1320 (1968).
 - [9] J. M. Dickey and A. Paskin, Phonon Spectrum Changes in Small Particles and Their Implications for Superconductivity, *Phys. Rev. Lett.* **21**, 1441 (1968).
 - [10] D. G. Naugle, J. W. Baker, and R. E. Allen, Evidence for a Surface-Phonon Contribution to Thin-Film Superconductivity: Depression of T_c by Noble-Gas Overlayers, *Phys. Rev. B* **7**, 3028 (1973).
 - [11] Y. Chen, A. A. Shanenko, and F. M. Peeters, Superconducting transition temperature of Pb nanofilms: Impact of thickness-dependent oscillations of the phonon-mediated electron-electron coupling, *Phys. Rev. B* **85**, 224517 (2012).
 - [12] L. Zhao, E. G. Arnault, A. Bondarev, A. Serebinski, T. F. Q. Larson, A. W. Draelos, H. Li, K. Watanabe, T. Taniguchi, F. Amet, H. U. Baranger, and G. Finkelstein, Interference of chiral Andreev edge states, *Nat. Phys.* **16**, 862 (2020).
 - [13] Y. Nagai, S. Hoshino, and Y. Ota, Critical temperature enhancement of topological superconductors: A dynamical mean-field study, *Phys. Rev. B* **93**, 220505 (2016).
 - [14] W. L. McMillan, Tunneling Model of the Superconducting Proximity Effect, *Phys. Rev.* **175**, 537 (1968).
 - [15] M. E. Zhitomirsky and T. M. Rice, Interband Proximity Effect and Nodes of Superconducting Gap in Sr_2RuO_4 , *Phys. Rev. Lett.* **87**, 057001 (2001).
 - [16] A. I. Buzdin, Proximity effects in superconductor-ferromagnet heterostructures, *Rev. Mod. Phys.* **77**, 935 (2005).
 - [17] M. D. Croitoru, A. A. Shanenko, Y. Chen, A. Vagov, and J. A. Aguiar, Microscopic description of surface superconductivity, *Phys. Rev. B* **102**, 054513 (2020).
 - [18] L. Chen, Y. Chen, W. Zhang, and S. Zhou, Non-gapless excitation and zero-bias fast oscillations in the LDOS of surface superconducting states, *Physica B: Condensed Matter* **646**, 414302 (2022).
 - [19] T. Giamarchi, M. T. Béal-Monod, and O. T. Valls, Onset of surface superconductivity, *Phys. Rev. B* **41**, 11033 (1990).
 - [20] Y. Bai, L. Zhang, X. Luo, A. A. Shanenko, and Y. Chen, Tailoring of interference-induced surface superconductivity by an applied electric field, *Phys. Rev. B* **108**, 134506 (2023).

- (2023).
- [21] M. Barkman, A. Samoilenka, and E. Babaev, Surface Pair-Density-Wave Superconducting and Superfluid States, *Phys. Rev. Lett.* **122**, 165302 (2019).
- [22] A. Samoilenka, M. Barkman, A. Benfenati, and E. Babaev, Pair-density-wave superconductivity of faces, edges, and vertices in systems with imbalanced fermions, *Phys. Rev. B* **101**, 054506 (2020).
- [23] Y. Chen, K.-J. Chen, J.-J. Zhu, and A. A. Shanenko, Emergence of surface superconductivity through interference in proximitized topological insulators, *Phys. Rev. B* **109**, 224514 (2024).
- [24] Y. Wang, G. Rai, S. Haas, and A. Jagannathan, Edge and corner superconductivity in a two-dimensional topological model, *Phys. Rev. B* **107**, 104507 (2023).
- [25] A. Benfenati, A. Samoilenka, and E. Babaev, Boundary effects in two-band superconductors, *Phys. Rev. B* **103**, 144512 (2021).
- [26] A. Samoilenka and E. Babaev, Boundary states with elevated critical temperatures in Bardeen-Cooper-Schrieffer superconductors, *Phys. Rev. B* **101**, 134512 (2020).
- [27] Y. Bai, Y. Chen, M. D. Croitoru, A. A. Shanenko, X. Luo, and Y. Zhang, Interference-induced surface superconductivity: Enhancement by tuning the Debye energy, *Phys. Rev. B* **107**, 024510 (2023).
- [28] K. Tanaka and F. Marsiglio, Anderson prescription for surfaces and impurities, *Phys. Rev. B* **62**, 5345 (2000).
- [29] P. G. de Gennes, *Superconductivity of Metals and Alloys* (Benjamin, New York, 1966).
- [30] Y. Chen, M. D. Croitoru, A. A. Shanenko, and F. M. Peeters, Superconducting nanowires: Quantum confinement and spatially dependent Hartree-Fock potential, *J. Phys.: Condens. Matter* **21**, 435701 (2009).
- [31] Y. Chen, Q. Zhu, M. Zhang, X. Luo, and A. Shanenko, Surface superconductor-insulator transition: Reduction of the critical electric field by Hartree-Fock potential, *Physics Letters A* **494**, 129281 (2024).
- [32] J. B. Ketterson and S. N. Song, *Superconductivity* (Cambridge, 1999).
- [33] Y. Chen, A. A. Shanenko, A. Perali, and F. M. Peeters, Superconducting nanofilms: Molecule-like pairing induced by quantum confinement, *Journal of Physics: Condensed Matter* **24**, 185701 (2012).
- [34] A. Perali, P. Pieri, L. Pisani, and G. C. Strinati, BCS-BEC Crossover at Finite Temperature for Superfluid Trapped Fermi Atoms, *Phys. Rev. Lett.* **92**, 220404 (2004).
- [35] P. Nozieres and S. Schmitt-Rink, Bose condensation in an attractive fermion gas: From weak to strong coupling superconductivity, *J. Low Temp. Phys.* **59**, 195 (1985).
- [36] Tinkham, *Introduction to Superconductivity* (McGraw-Hill, Inc., 1996).
- [37] Y. Wang, G. Rai, C. Matsumura, A. Jagannathan, and S. Haas, Superconductivity in the Fibonacci chain, *Phys. Rev. B* **109**, 214507 (2024).